Multiobjective optimization of multi-cell sections for the crashworthiness design

Article *in* International Journal of Impact Engineering · November 2008

DOI: 10.1016/j.ijimpeng.2007.09.003

5 authors, including:

Shujuan Hou
Hunan University
70 PUBLICATIONS **3,588** CITATIONS
SEE PROFILE

Qing Li
The University of Sydney
528 PUBLICATIONS **24,787** CITATIONS
SEE PROFILE

Xujing Yang
Hunan University
110 PUBLICATIONS **3,248** CITATIONS
SEE PROFILE

Wei Li
CCS Haryana Agricultural University
1,050 PUBLICATIONS **75,349** CITATIONS
SEE PROFILE

Available online at www.sciencedirect.com
ScienceDirect
ELSEVIER
International Journal of Impact Engineering 35 (2008) 1355–1367
INTERNATIONAL JOURNAL OF IMPACT ENGINEERING
www.elsevier.com/locate/ijimpeng

Multiobjective optimization of multi-cell sections for the crashworthiness design

Shujuan Hou[a], Qing Li[b,*], Shuyao Long[a], Xujing Yang[a], Wei Li[b]

[a]State Key Laboratory of Advanced Design and Manufacturing for Vehicle Body, Hunan University, Changsha, Hunan 410082, PR China
[b]School of Aerospace, Mechanical and Mechatronic Engineering, The University of Sydney, Sydney, NSW 2006, Australia

Received 3 August 2006; received in revised form 13 September 2007; accepted 20 September 2007
Available online 20 March 2008

Abstract

Plastic deformation of structures absorbs substantial kinetic energy when impact occurs. For this reason, energy-absorbing components have been extensively used in the structural design of vehicles to intentionally absorb a large portion of crash energy to reduce the severe injury of occupants. On the other hand, high peak crushing force may to a certain extent indicate the risk of structural integrity and biomechanical damage of occupants. For this reason, it is of great significance to maximize the energy absorption and minimize the peak force by seeking for optimal design of these components. This paper aims to design the multi-cell cross-sectional thin-walled columns with these two crashworthiness criteria. An explicit finite element analysis (FEA) is used to derive higher-order response surfaces for these two objectives. Both the single-objective and multi-objective optimizations are performed for the single, double, triple and quadruple cell sectional columns under longitudinal impact loading. A comparative analysis is consequently given to explore the relationship between these two design criteria with the different optimization formulations.

Keywords: Multi-objective optimization; Crashworthiness; Multi-cell; Impact; Response surface method

1. Introduction

A severe crushing-induced kinematic deformation and material damage do not always imply a negative feature of design in engineering practice. Taking a vehicle as an example, some structural components have been set up to deliberately generate substantial deformation and damage for a purpose of absorbing as much kinetic energy as possible in case impact occurs such that severe impact-induced occupant's injury could be avoided. One of other major concerns in crash is the peak force generation, which may determine structural integrity of vehicle and biomechanical responses of occupants. Hence, these energy absorption components are also anticipated to have a minimum peak force. As such, crashworthiness criteria have become a special topic in design research and have been particularly prevalent in the automotive industry nowadays to ensure the vehicle structural integrity and more importantly the occupant safety in an event of crash [1–3].

However, a major challenge remains how to seek for an optimal sectional configuration for the energy-absorption components such that the highest crashworthiness performance can be attained. In spite of its obvious practical significance, such an optimization problem involves high nonlinearities of material and geometry, which have not been effectively addressed unless some empirical closed-form solutions or surrogate model techniques were adopted [4,5]. In the latter, the response surface method (RSM) gains extensive popularity as various computational crashing simulation techniques are established, and its applications in crashworthiness design have been substantially explored by a number of researchers, e.g. Lee et al. [6], Avalle et al. [7], Chiandussi et al. [8], Kim [9], Jansson et al. [10], Lee et al. [11] and Forsberg and Nilsson [12,13]. It is noted that in these earlier studies, exhaustive attention has been paid to such simpler and more conventional thin-walled sectional structures as squared or circular tubes [6] and their tapered variations [7,8].

*Corresponding author. Tel.: +61 2 9351 8607; fax: +61 2 9351 7060.
E-mail address: Q.Li@usyd.edu.au (Q. Li).

0734-743X/$ - see front matter © 2007 Elsevier Ltd. All rights reserved.
doi:10.1016/j.ijimpeng.2007.09.003

Along with development of various high-performance alloys and composite materials, more complex sectional structures have become commercially available. In the context, aluminum and its alloys signify one class of promising energy-absorbing materials due to its relative high ratio of functionality to weight, which has been widely adopted in the structural design of vehicles. Furthermore, aluminum is of excellent formability and almost any realistically shaped multiply-connected cross-sectional can be produced by an extrusion process, which provides a great possibility to economically implement a specific design of sectional configuration. As more and more aluminum thin-walled columns are used in energy-absorption structures, it becomes increasingly important to optimize the sectional parameters to achieve the best possible crashworthiness when impact occurs.

As a relatively new class of sectional configuration, multi-cell thin-walled structures exhibit exceptionally high capacity of energy absorption, which have recently drawn increasing attention in the research community and automotive industry. In this regard, Chen et al. [14] systemically investigated a relative performance of single-, double- and triple-celled columns. In their study, notwithstanding the recognition of importance to wall thickness, it remains unclear what the best value is, so does the sectional width for a given constraint of mass. To increase the energy absorption, Kim developed a novel type of section with various squared cells attached to the corner [9]. An empirical objective function is constructed in terms of mean crushing force and final displacement, which allows determining their analytical derivatives with respect to the size variables chosen. Such new designs demonstrated a considerably higher crashworthiness than those more conventional designs by Chen et al. [14]. Although these studies showed great promise, there is a fundamental lack of thorough design studies on multi-celled columns in particular when multiple crashworthiness criteria, e.g. specific energy absorption (SEA) and peak crushing force, are involved.

On the other hand, multi-objective optimization, as a more practical design methodology, aims at addressing a number of design criteria, which has become an attractive research topic in crashworthiness design recently [3,15–17]. Although a variety of mathematical models and algorithms has been available so far, it is by no means easy to achieve various crashworthiness objectives simultaneously. Often, some of these criteria conflict each other, which to a certain stage, any further improvement in one criterion must worsen one or more other criteria [3]. In this regard, two typical approaches are considered feasible in practice. The simplest method is to convert the multi-objective optimization to a single-objective problem, in which a "primary" criterion is selected as an objective function whereas other less important criteria are prescribed as functional constraints [18,19]. This treatment enables us to use a range of well-established constrained mathematical programming or evolutionary algorithms, thereby generating a single solution to the problem. However, it is not easy even for an experienced design engineer to identify a predominant objective from a long list of design requirements [5]. Furthermore, there may be some difficulty to adequately prescribe constraints to those secondary criteria. For this reason, it may be more appropriate to impose the problem in a multi-objective optimization framework, where multiple design criteria are addressed as the objectives for optimization, simultaneously. Unlike the single-objective formulation, a multi-objective framework normally generates a group of solutions in a Pareto sense. As such, a more thorough understanding of the optimal design space may be established to allow making a better design decision [5,17,20]. But the challenge remains how to formulate a unified multi-objective optimization problem to facilitate use of various mathematical programming [5], and how to justify an optimal design from a Pareto frontier. A very interesting yet practical problem is how these two above-mentioned approaches develop a multi-objective crashworthiness design for the multi-celled sectional structures.

The present study aims at maximizing the energy absorption efficiency and minimizing the peak crushing force for thin-walled aluminum structures, where cross-sectional sizes of single-, double-, triple- and quadruple-cell columns are taken into account in an explicit finite element (FE) framework. A high-order response surface (RS) is constructed to precisely establish the relationship between the objective functions of the SEA as well as peak crushing force and the geometrical design variables of the sectional configurations considered. In this paper, multicriteria design is formulated as both the constrained single-objective and multiple-objective optimization problems. The comparative studies will show how these two criteria interact with each other in different optimization formulations and how a compromise can be made for an optimal design.

2. Design methodology

2.1. Definition of crashworthiness optimization problem

The structural impact problem is one class of geometry and material nonlinear problems. Therefore, the total strain energy absorbed by the structure during the deformation includes not only the elastic component but also the plastic strain energy. In a FE framework, the total strain energy can be computed in a structural volume of V as

$$E_{\text{total}} = \int_V A(\varepsilon)\,\mathrm{d}V, \tag{1}$$

where $A(\boldsymbol{\varepsilon})$ represents the total strain energy density of the structure concerned. It is expected that the optimized sectional thin-walled column is able to absorb as much strain energy as possible in a unit structural weight, which is defined as the SEA (in a unit of kJ/kg) [9] shown in Eq. (2).

$$\text{SEA}(\mathbf{x}) = \frac{E_{\text{total}}}{m}, \tag{2}$$

where m is the total mass of the structure considered.

On the other hand, the peak crushing force is sometimes considered one of the critical design objectives to prevent the occupant's body from severe biomechanical injury [21,22]. Although the mean crushing force of the multi-cell square column can be approximately expressed by using the closed-form solutions [14], the peak force is found very difficult to be formulated in terms of geometric design variables analytically. More importantly, the crushing force is time-dependent, whose peak may occur at different time steps in different designs. This makes the exploitation of traditional FE-driven sensitivity analysis techniques very challenging. Nevertheless, in a FE-based RSM framework, the true peak crushing force $P(\mathbf{x})$ can be approximated in terms of various basis functions and their combinations, numerically.

To account for these two different design criteria, the optimization problem can be formulated in the following forms:

(1) The single-objective optimization design with a major concern in the energy absorption capacity of structure as

$$\begin{cases} \text{Maximize} & f_1 = \text{SEA}(\mathbf{x}) \\ \text{s.t.} & P(\mathbf{x}) \leqslant P_{\text{const.}}, \\ & \mathbf{x}^{\text{L}} \leqslant \mathbf{x} \leqslant \mathbf{x}^{\text{U}} \end{cases} \tag{3a}$$

and in the peak crushing force as

$$\begin{cases} \text{Minimize} & f_2 = P(\mathbf{x}) \\ \text{s.t.} & \text{SEA}(\mathbf{x}) \geqslant \text{SEA}_{\text{const.}}, \\ & \mathbf{x}^{\text{L}} \leqslant \mathbf{x} \leqslant \mathbf{x}^{\text{U}}, \end{cases} \tag{3b}$$

respectively, where $P_{\text{const.}} = 70\,\text{kN}$ and $\text{SEA}_{\text{const.}} = 10\,\text{kJ/kg}$ are given as the constraints of peak crushing force and SEA, respectively [22,23]. $\mathbf{x}^{\text{L}} = (x_1^{\text{L}}, x_2^{\text{L}}, \ldots, x_k^{\text{L}})$ and $\mathbf{x}^{\text{U}} = (x_1^{\text{U}}, x_2^{\text{U}}, \ldots, x_k^{\text{U}})$ stand for the lower and upper bounds of these k design variables, respectively.

(2) Multi-objective optimization can be formulated in different fashions. One of the typical designs account for different criteria in terms of weights to provide different emphasis, as

$$\begin{cases} \text{Minimize} & F_w = (1-w)\,\dfrac{f_1^*}{f_1} + w\,\dfrac{f_2}{f_2^*} \\ \text{s.t.} & w \in [0,1] \text{ and } \mathbf{x}^{\text{L}} \leqslant \mathbf{x} \leqslant \mathbf{x}^{\text{U}}, \end{cases} \tag{4}$$

where f_1^*, f_2^* are the given normalizing values of $f_1 = \text{SEA}(\mathbf{x})$ and $f_2 = P(\mathbf{x})$, respectively, for the multi-objective optimization design [3,15]. w is the weight factor for a purpose to emphasize different importance of these two objectives [20].

Unlike the linear weighted average as presented in Eq. (4), an alternative formulation of multi-objective optimization adopts the geometrical average of "efficiency coefficients" (d_{SEA} and d_{P}) of these two different objectives, as

$$\begin{cases} \text{Maximize} & F_{\text{g}} = \sqrt{d_{\text{SEA}} d_{\text{P}}} \\ \text{s.t.} & \mathbf{x}^{\text{L}} \leqslant \mathbf{x} \leqslant \mathbf{x}^{\text{U}}, \end{cases} \tag{5}$$

in which the efficiency coefficients can be defined in two different ways. To maximize SEA, the efficiency coefficient d_{SEA} is calculated in terms of a relative distance to the lower bound, as

$$d_{\text{SEA}} = \frac{f_1(\mathbf{x}) - f_1^{\text{L}}}{f_1^{\text{U}} - f_1^{\text{L}}} \tag{6}$$

and to minimize the peak crushing force the efficiency coefficient d_{P} is calculated as

$$d_{\text{P}} = 1 - \frac{f_2(\mathbf{x}) - f_2^{\text{L}}}{f_2^{\text{U}} - f_2^{\text{L}}}, \tag{7}$$

where f^{L} and f^{U} represent the lower and upper bounds of the objective function in the design space, respectively. The efficiency coefficients d_{SEA} and d_{P} are the functions of the design variables, and they vary in the range of $0 \leqslant d_{\text{SEA}}, d_{\text{P}} \leqslant 1$. When overall efficiency coefficient $F_{\text{g}} = 1$, the corresponding objective function reaches its ideal (optimal) solution, whereas $F_{\text{g}} = 0$ indicates the worst solution.

2.2. Response surface method

RSM is considered effective in the design optimization problems involving either high mathematical complexity of sensitivity analysis like strain energy in contact-impact [6–10] or difficulty of analytical expression of physical quantity like peak crushing force. In this paper, the specific objective functions, like SEA in Eq. (2) or the peak crushing force, are numerically approximated in terms of basis functions [4,24,25] as

$$\tilde{y}(\boldsymbol{x}) = \boldsymbol{\alpha}^{\text{T}} \boldsymbol{\varphi}(\mathbf{x}), \tag{8}$$

where α_j $(j = 1, 2, \ldots, N)$ in vector $\boldsymbol{\alpha}$ denotes the jth unknown coefficient corresponding to the jth basis function $\varphi_j(\mathbf{x})$. In general, the selection of basis function should ensure adequate accuracy and convergence [4,8]. In this paper, a full set of the 4th order of polynomial functions is adopted, as follows,

$$\begin{aligned} &1, x_1, x_2, \ldots, x_n, x_1^2, x_1x_2, \ldots, x_1x_n, \ldots, x_n^2, x_1^3, \\ &x_1^2x_2, \ldots, x_1^2x_n, x_1x_2^2, \ldots, x_1x_n^2, \ldots, x_n^3, x_1^4, x_1^3x_2, \ldots, x_1^3x_n, \\ &x_1^2x_2^2, \ldots, x_1^2x_n^2, \ldots, x_1x_2^3, \ldots, x_1x_n^3, \ldots, x_n^4. \end{aligned} \tag{9}$$

To determine the unknown parameters $\boldsymbol{\alpha} = (\alpha_1, \alpha_2, \ldots, \alpha_N)^{\text{T}}$ in the response function Eq. (8), a large number of FE analyses (FEAs) are needed at some selected sampling points $\mathbf{x}^{(i)} (i = 1, 2, \ldots, M)(M > N)$, which will enable one to construct a second norm of error $E(\boldsymbol{\alpha})$ between the objective y and the response function $\tilde{y}$ defined

in Eq. (8) as

$$E(\boldsymbol{\alpha}) = \boldsymbol{\varepsilon}^{\mathrm{T}}\boldsymbol{\varepsilon} = (\boldsymbol{y} - \boldsymbol{\Phi}\boldsymbol{\alpha})^{\mathrm{T}}(\boldsymbol{y} - \boldsymbol{\Phi}\boldsymbol{\alpha}), \tag{10}$$

where objective vector $\boldsymbol{y} = (y^{(1)}, y^{(2)}, \ldots, y^{(M)})^{\mathrm{T}}$ and response vector $\boldsymbol{\Phi}\boldsymbol{\alpha}$ are, respectively, obtained from FE analyses and the response function, matrix $\boldsymbol{\Phi}$ denotes the values of basis functions that are evaluated at these M sampling points as

$$\boldsymbol{\Phi} = \begin{bmatrix} \varphi_1(\mathbf{x}^{(1)}) & \cdots & \varphi_N(\mathbf{x}^{(1)}) \\ \vdots & \ddots & \vdots \\ \varphi_1(\mathbf{x}^{(M)}) & \cdots & \varphi_N(\mathbf{x}^{(M)}) \end{bmatrix}. \tag{11}$$

The least-square method is then applied to minimize the error norm $E(\boldsymbol{\alpha})$ in Eq. (10), and the unknown parameter $\boldsymbol{\alpha}$ is consequently evaluated as

$$\boldsymbol{\alpha} = (\boldsymbol{\Phi}^{\mathrm{T}}\boldsymbol{\Phi})^{-1}(\boldsymbol{\Phi}^{\mathrm{T}}\boldsymbol{y}). \tag{12}$$

By substituting Eq. (12) to Eq. (8), the expression of $\tilde{y}(x)$ can be fully determined, which establishes an approximate analytical relationship between the objective function and the design variables.

2.3. Design of Experiment (DoE)

DoE provides a means to selection of the sampling points in the design space in a more efficient way. There are many different experimental design methods available, such as the factorial, Koshal, composite, Latin Hypercube and D-optimal design, etc. [4,5,24,26]. Here we made use of the "factorial design" for its uniformity of sampling in an unknown design space.

Specifically, a r^s full factorial design generates a mesh of sampling points (an s-dimensional hypercube) consisting of r points spaced at regular intervals in each variable direction. To create an approximation of order r, at least $(r+1)^s$ factorial designs are needed [26]. In this study, $r = 4$ and $s = 2$ are taken.

2.4. Error evaluation of the surrogate model

The numerical errors in the RS model can be caused by the selection of basis functions, selection of sampling points and the least square. To measure the degree of approximation to the FEA results, the relative error (RE) can be evaluated as

$$\mathrm{RE} = \frac{\tilde{y}(\mathbf{x}) - y(\mathbf{x})}{y(\mathbf{x})}, \tag{13}$$

where $\tilde{y}(\mathbf{x})$ represents approximation based on the response surface established and $y(\mathbf{x})$ denotes the numerical solution directly from FEA.

In addition to this, statistical analysis techniques such as analysis of variance [3,27] can be used to check the fitness of an RS model so as to identify the effects of design variables on the responses. The typical statistical parameters used for evaluating the model fitness are the F statistics in terms of R^2, adjusted R^2_{adj} and root of mean-squared error (RMSE), respectively, as [5,27]

$$F = \frac{(\mathrm{SST} - \mathrm{SSE})/p}{\mathrm{SSE}/(M - p - 1)}, \tag{14}$$

$$R^2 = 1 - \mathrm{SSE}/\mathrm{SST}, \tag{15}$$

$$R^2_{\mathrm{adj}} = 1 - (1 - R^2)\frac{M - 1}{M - p - 1}, \tag{16}$$

$$\mathrm{RMSE} = \sqrt{\frac{\mathrm{SSE}}{M - p - 1}}, \tag{17}$$

where p is the number of nonconstant terms in the RS model, M is the number of design sampling points, SSE and SST are the sum of squared errors and the total sum of squares, respectively, calculated as

$$\mathrm{SSE} = \sum_{i=1}^{M}(y_i - \tilde{y}_i)^2, \tag{18}$$

$$\mathrm{SST} = \sum_{i=1}^{M}(y_i - \bar{y}_i)^2, \tag{19}$$

where $\bar{y}_i$ is the mean value of FEA result y_i.

It should be pointed out, however, that these measures may not be completely independent on each other and there may be some interconnections between them. Generally speaking, the larger the values of R^2 and R^2_{adj}, and the smaller the value of RMSE, the better the fitness [3,26].

In this study, a five-level full factorial design was used for sampling [3], which resulted in 25 (5^2) evenly distributed design points in the design range of t and a. In order to justify the selection of design points and the orders of the 4th polynomials, we firstly take the single-cell column as an example to construct the different polynomial RS models with the orders ranging from 1 to 5, and then assess their accuracies using Eqs. (13)–(19). The results of approximations are summarized in Table 1. The larger values of R^2 and R^2_{adj}, as well as the smaller values of RMSE and RE, indicate a better fitness of the RS model. Table 1 clearly shows that of all these 5 RS models, the quartic polynomial function consistently provides the best approximation. The data also validate the adequacy of factorial selection of such evenly distributed 25 design points in the design domain [3].

Table 1
Accuracy of different polynomial RS models for the single-cell case

RS model	R^2	R^2_{adj}	RMSE	RE interval (%)
Linear polynomial	0.9923	0.9916	0.2862	[−14.01, 7.21]
Quadratic polynomial	0.9993	0.9992	0.0904	[−2.95, 2.89]
Cubic polynomial	0.9995	0.9992	0.0859	[−1.67, 2.89]
Quartic polynomial	1.0000	0.9999	0.0326	[−0.67, 1.03]
Quintic polynomial	−4.5855	−32.5130	18.0811	[32.95, 191.81]

The same methods can be applied to validate the RS models and design points selections of the other three column structures, where the same conclusion can be obtained.

3. Formulation of design problems

3.1. Definition of design models

The structures considered in this study are the thin-walled columns with multi-celled square sections, in which the single-, double-, triple- and quadruple-celled configurations are investigated, as illustrated in Fig. 1. The width a of the cross-sections and the thickness t of the thin wall are chosen as the design variables, and the constraints of these two design parameters are given as $60\,\text{mm} \leqslant a \leqslant 100\,\text{mm}$ and $1.4\,\text{mm} \leqslant t \leqslant 3.0\,\text{mm}$, respectively, which are set for all these four configurations in Fig. 1. The length L of the thin-walled column is a constant of 400 mm.

In the optimization, these four design configurations are taken into account under the same longitudinal impact loading condition, as depicted in the computational models in Fig. 2, where the thin-walled column structures impact onto a rigid wall with 10 m/s initial velocity over 20 ms of crash time. A 500 kg lumped mass is attached to all the four configurations on the free end of the columns.

The thin-walled structures are made of the aluminum alloy AA6061-T4 with the material properties of density $\rho = 2.7 \times 10^3\,\text{kg/m}^3$, Young's modulus $E = 70.0\,\text{GPa}$, Poisson's ratio $v = 0.28$, yield stress $\sigma_s = 110.3\,\text{MPa}$, tangent elastic modulus $E_t = 450\,\text{MPa}$, ultimate strength $\sigma_u = 213.0\,\text{MPa}$ and elongation 19% [14]. A plastic kinematic hardening material model 3 in LS-DYNA [28] is adopted for simulating AA6061-T4 in this paper [13]. As the aluminum is insensitive to the strain rate [9], its rate dependence is neglected in the FE modeling. In order to calculate the energy absorption per unit mass of structure, the total structural masses are calculated, respectively, as

$$\begin{aligned} &\text{Single-cell :} && m = 4\rho Lt(a - t),\\ &\text{Double-cell :} && m = \rho Lt(5a - 6t),\\ &\text{Triple-cell :} && m = \rho Lt(6a - 8t),\\ &\text{Quadruple-cell :} && m = \rho Lt(6a - 9t). \end{aligned} \tag{20}$$

In this study, the four-node shell element with bending and membrane capacities introduced by Belytschko et al. [29] is employed. The rigid-wall definition is given by using the internal rigid-wall feature in LS-DYNA [28]. A single surface contact algorithm is used to account for the contact between lobes and internal self-contact of the shell elements during deformation.

3.2. Response surface models

Table 1 has shown that the full quartic polynomial function provides a best approximation. Therefore, the 4th-order response functions of SEAs and peak crushing forces for these four columns are established for different cell configurations and the expressions of SEA($\mathbf{x}$) and $P(\mathbf{x})$ are given in Eqs. (A.1)–(A.4) in Appendix A. The RS of SEA and peak crushing force are, respectively, depicted in Figs. 3(a) and (b).

The maximum relative errors of these response functions defined in Eqs. (A.1)–(A.4) in Appendix A are in a range of 1–3% in these four sectional configurations, which are considered fairly adequate for the design optimization purpose. By plotting the RS, a certain extent of nonlinearities of the response functions (both SEA and peak crushing force) is observed in Figs. 3(a) and (b). It appears that the SEA RS and peak crushing force RS of 1-cell, 2-cell and 3-cell cases behave monotonically over the design domain as Figs. 3(a) and (b), while a 4-cell case has the nonmonotonic surfaces in aspects of SEA and peak

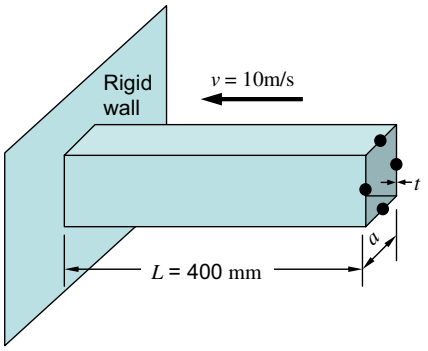

Fig. 2. The longitudinal impact model with loading condition.

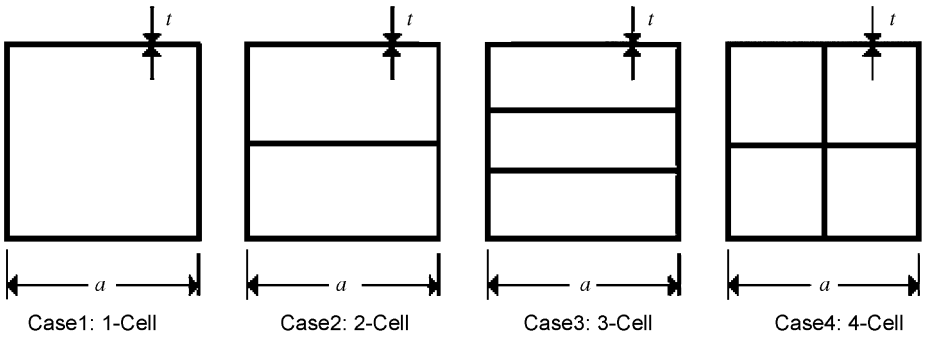

Fig. 1. The configurations of multi-cell sections.

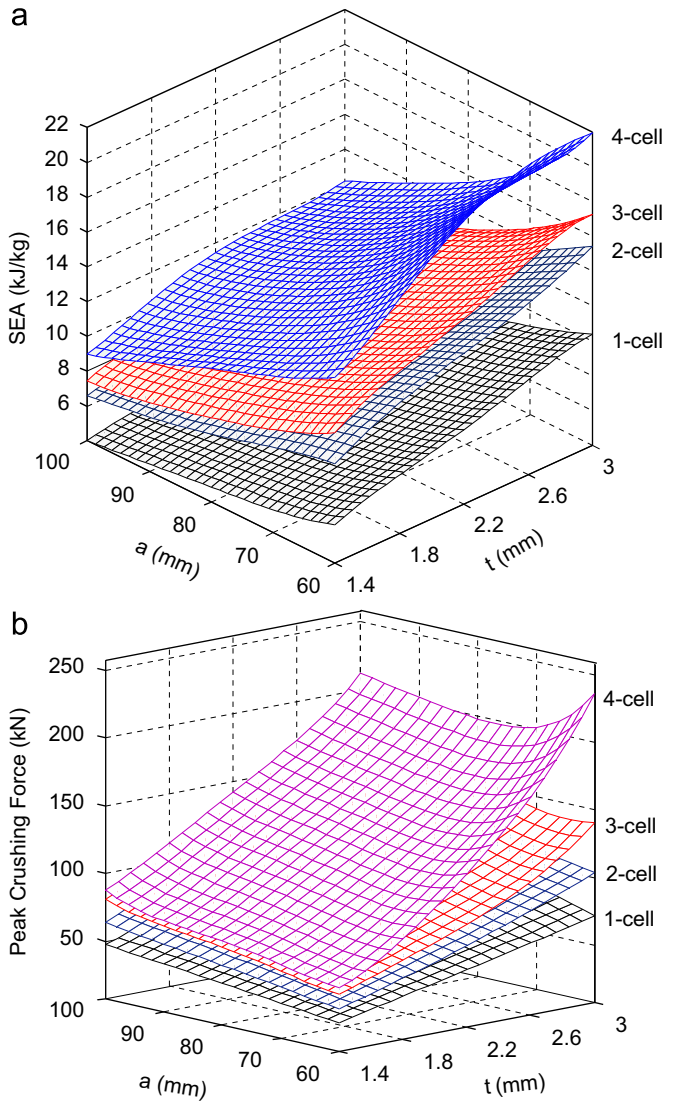

Fig. 3. The response surfaces under the longitudinal impact: (a) SEA response surfaces; (b) peak crushing force response surfaces.

crushing force as Figs. 3(a) and (b). Our numerical experiments showed that the 4th-order polynomial basis function seems necessary to attain an adequate fitting accuracy for all these four design cross-sections (<3%). It should be pointed out, however, that a higher-order basis function is not always advocated since the higher the order, the more the sampling points needed, and subsequently the higher the computational cost required in general.

3.3. Validation of the response surface models

In the literature, some close-form solutions to the SEA and peak crushing force have been derived from either experimental tests or continuum mechanics theory for the single-cell square column. For example, the closed form of $\mathrm{SEA} = 85.5(t/a)^{2/3}$ from Wierzbicki and Abramowicz's theory of plastic crushing of square columns [30,31], and the close form of the peak force $= 44at$ based on Stowell theory of plastic buckling of plates and columns [6]. Fig. 4 clearly shows the comparisons between the FE-based RS and the close-form surfaces. It is noted that the quartic RS correlate to these close-form solutions fairly well.

It is noted that the close-form solutions provide much shorter mathematical formulae. Nevertheless, the RS consist of simple polynomials, which provide flexibility to formulate different objectives for varying sectional complexity of columns in a consistent fashion. The close-form solutions to SEA and peak crushing force have been available mainly for simple columns in the literature. To facilitate formulating the solutions for the various multi-celled columns, the RS technique is thus adopted in this paper.

4. Results of design optimization

4.1. Constrained single-objective optimization

With the explicit formulation of SEA(**x**) and $P(\mathbf{x})$ (Eqs. (A.1)–(A.4)), the two constrained single-objective optimization problems are more specifically defined as

$$\begin{cases} \text{Maximize} & f_1 = \mathrm{SEA}(t,a) \\ \text{s.t.} & P(t,a) \leqslant 70\,\text{kN}, \\ & 1.4\,\text{mm} \leqslant t \leqslant 3.0\,\text{mm}, \\ & 60\,\text{mm} \leqslant a \leqslant 100\,\text{mm} \end{cases} \tag{21a}$$

and

$$\begin{cases} \text{Minimize} & f_2 = P(t,a) \\ \text{s.t.} & \mathrm{SEA}(t,a) \leqslant 10\,\text{kJ/kg} \\ & 1.4\,\text{mm} \leqslant t \leqslant 3.0\,\text{mm}, \\ & 60\,\text{mm} \leqslant a \leqslant 100\,\text{mm}. \end{cases} \tag{21b}$$

Fig. 3 also shows a broad range of changes in these objective functions, which points to the potential merit of design optimization. By using a constrained nonlinear multivariable optimization function in MATLAB (named "fmincon"), the optimal results of Eqs. (21a) and (21b) can be obtained as summarized in Tables 2 and 3, respectively. It is known that the optimal sectional widths and wall thicknesses appear consistent for the single-, double- and triple-cell columns due to the quasi-monotonic SEA and the peak force response functions shown in Fig. 3, while the optimum is attained in a convex crest in the quadruple-cell column.

Specifically, Table 2 presents the results of maximizing SEA with the peak crushing force constraint, and Table 3 gives the results of minimizing peak crushing force with the SEA constraint, from which it can be found that the side length $a = 60\,\text{mm}$ (its lower bound) is an optimum for these four different layouts in both the SEA design and the peak crushing force designs. However, the optimal wall thickness t varies for different design problems and different sectional configurations. In addition, it can be known from Table 2 that an increase in the number of cells will lead to an increase in SEA, which can also be seen in

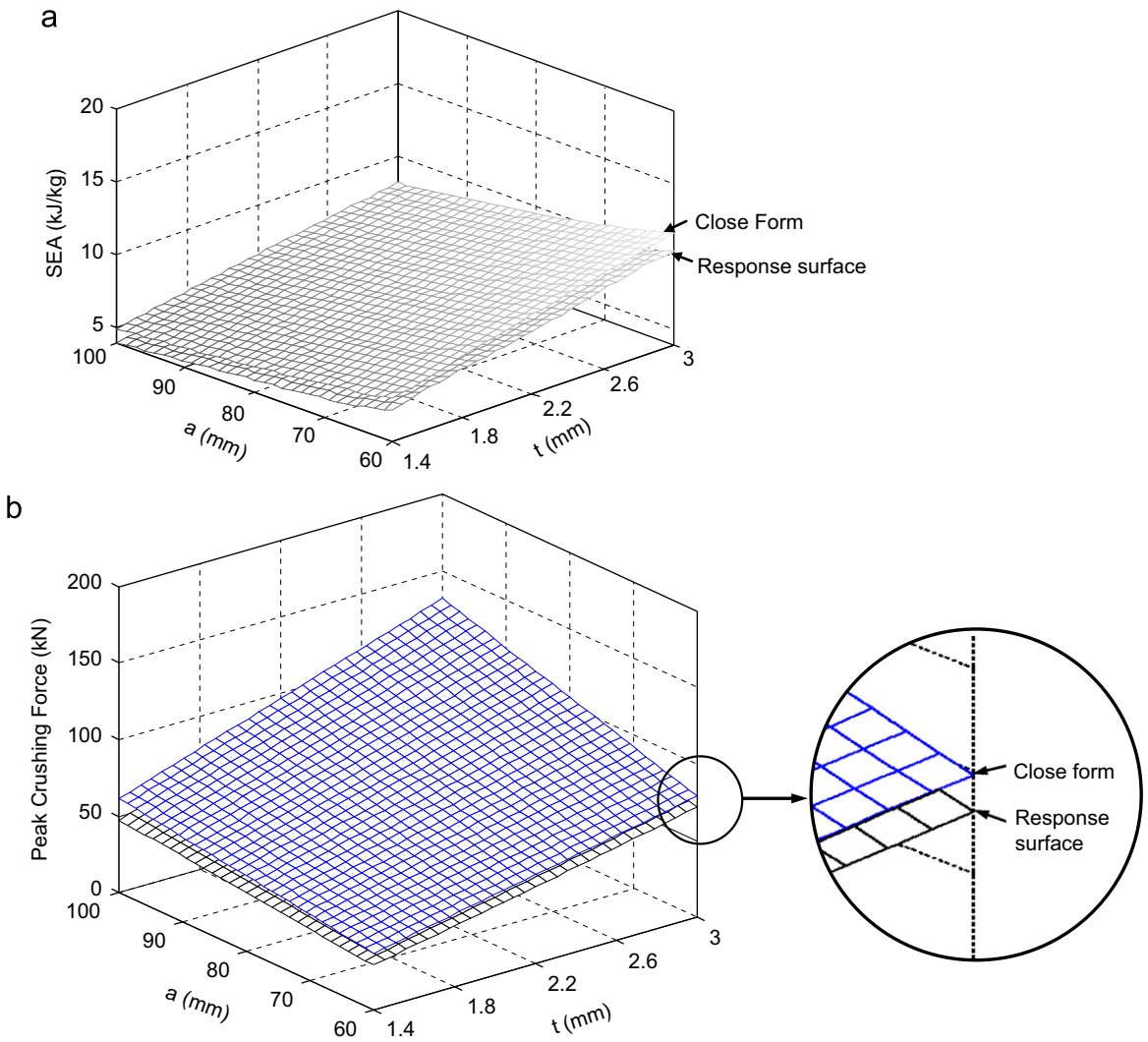

Fig. 4. Comparisons between the response surface and close form solution based on Wierzbicki and Abramowicz theory (SEA) and Stowell theory (peak force): (a) SEA comparisons; (b) peak crushing force comparisons.

Table 2
Optimization results of maximizing SEA with peak crushing force constraint

Type of cross-section	Optimal design variables (mm)	Max. SEA (kJ/kg)	P value (kN)
Single cell	$t = 2.89$, $a = 60$	10.22	69.02
Double cell	$t = 2.24$, $a = 60$	12.76	69.68
Triple cell	$t = 1.88$, $a = 60$	13.60	69.62
Quadruple cell	$t = 1.65$, $a = 60$	16.33	69.60

Table 3
Optimization results of minimizing peak crushing force with SEA constraint

Type of cross-section	Optimal design variables (mm)	Min. P (kJ/kg)	SEA value (kN)
Single cell	$t = 2.83$, $a = 60$	67.36	10.09
Double cell	$t = 1.45$, $a = 60$	40.89	10.00
Triple cell	$t = 1.4$, $a = 60$	49.79	11.50
Quadruple cell	$t = 1.4$, $a = 60$	54.48	14.68

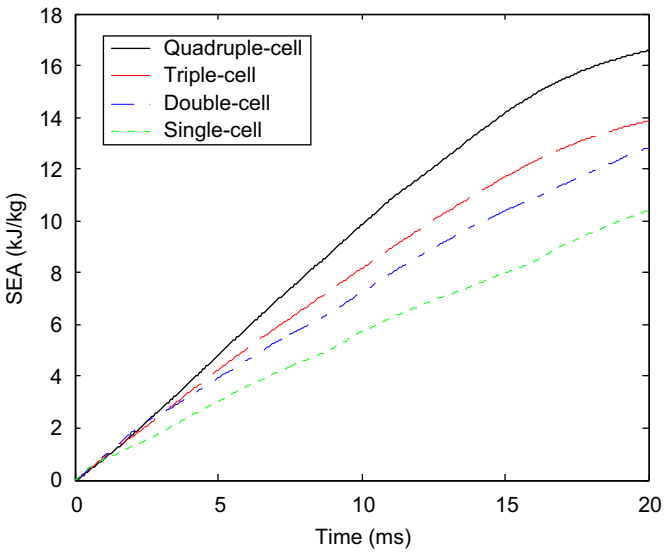

Fig. 5. Structural SEA *vs* time curves with the optimal design variables in Table 2.

Fig. 5. But in Table 3 and Fig. 6, the minimization of the peak crushing force with the constraint of SEA, does not appear to have such a consistent variation. From Fig. 5, it also can be seen that time has a definite effect on the rate of energy absorption. In general, the longer the time, the lower the energy absorption rate. Furthermore, the multi-cell configurations have higher SEA rate than the single-cell section over the entire time domain considered, which also shows that the multi-cell configurations perform better.

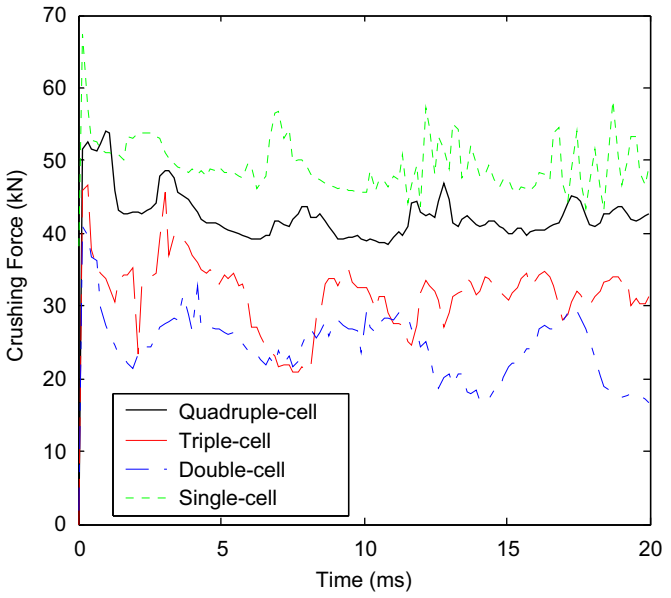

Fig. 6. Peak crushing force *vs* time curves with the optimal design variables in Table 3.

The curves of the peak crushing force *vs* time are plotted in Fig. 6 with the optimal designs in Table 3. It is noted that there is no regularity for the four minimum peak force levels. It is evident that the peak crushing forces reach a minimum when the design variable a is in the lower bound ($a = 60$ mm). Moreover, it is seen that the peak forces occur near the starting point of crash under longitudinal loading.

It is interesting to note from design analysis that the structure with a less ratio of sectional width to wall thickness often absorbs more strain energy per unit weight. This tendency can be observed from Fig. 7, where the fitting curves of SEA *vs* the ratio of sectional width to wall thickness are plotted. It should be pointed out that the asterisks in Fig. 7 stand for the FEA results at different sample points. For different sets of a and t, there may be the same or a close value of the ratio, but they can signify quite different SEAs. Taking the designs of $a = 90$ mm, $t = 2.6$ mm and $a = 100$ mm, $t = 3.0$ mm as an example, the ratios a/t are 34.615 and 33.333, respectively, which appears fairly close to each other in their horizontal coordinate, but have sizable differences in their vertical coordinates, when plotted in Fig. 7.

Fig. 8 shows the deformed configurations corresponding to the optimized columns in Table 2, from which it can be seen that all the structures develop stable folding deformation patterns. It is noted that the single-cell cross-sectional

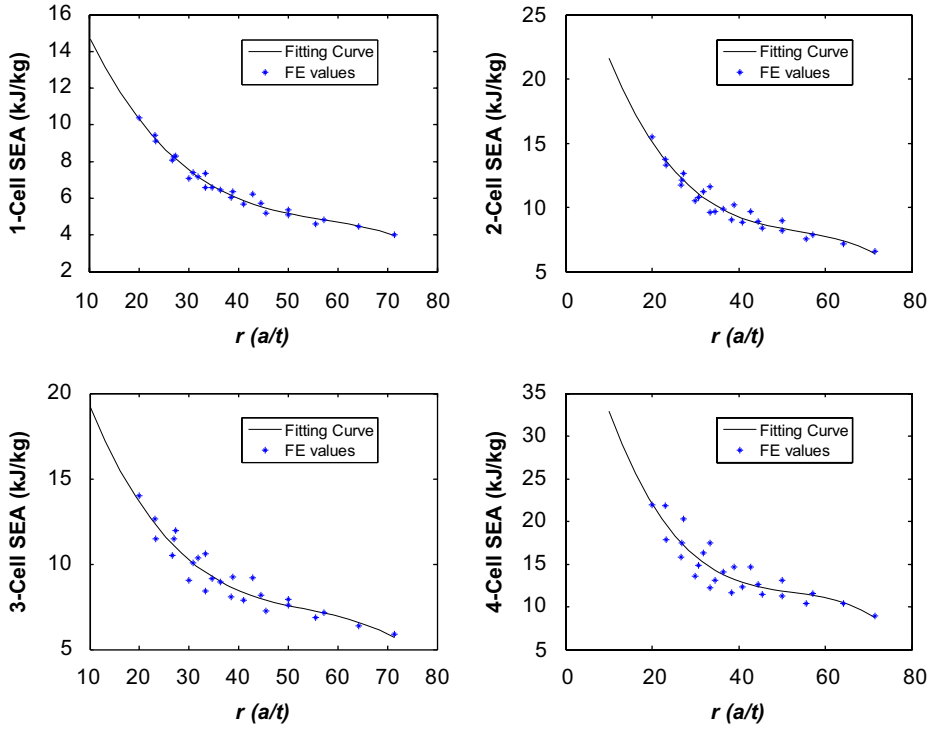

Fig. 7. Influences of the ratio $r = a/t$ on SEA under the longitudinal impact.

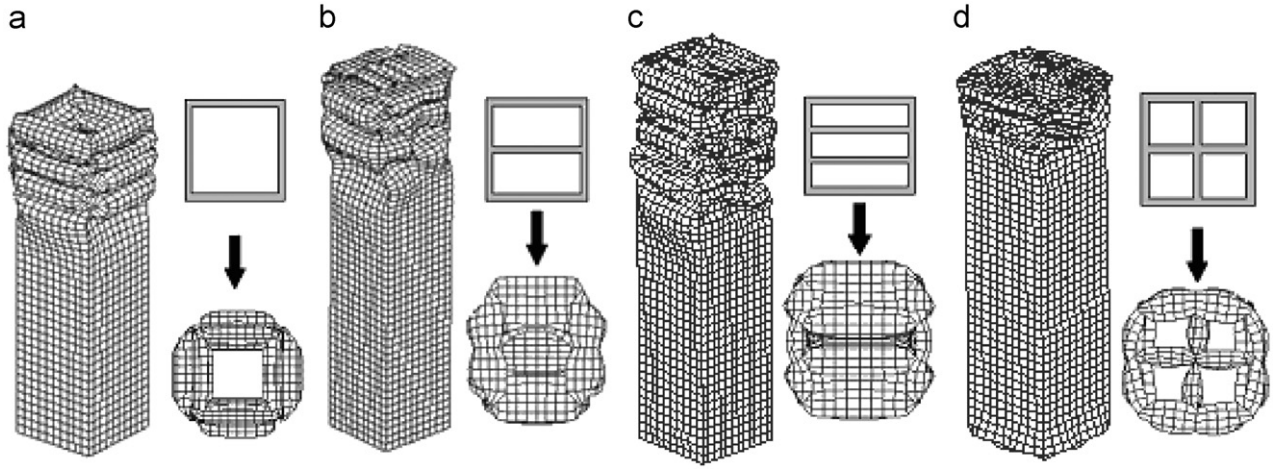

Fig. 8. Deformation of optimal sectional columns under the longitudinal impact. (a) Single cell; (b) double cell; (c) triple cell and (d) quadruple cell.

profile develops a most typical progressive folding pattern, followed by the double-, triple- and quadruple-cell cases. It should be recognized that the number of "corner" elements on a tube's cross-section determines, to a certain extent, the efficiency of the energy absorption [30,31], which more or less accounts for why SEA of the quadruple-cell profile is the highest of all these four sections.

4.2. Multi-objective optimization

Although optimizing one criterion whereas treating another as a constraint does generate meaningful results, it lacks an important feature of exploring the interaction of these criteria. From a practical point of view, multi-objective design appears more meaningful [32]. In this paper, we defined a multi-objective optimization of maximizing SEA and minimizing peak crushing force (P) by using the linear weighted average and geometrical average methods, respectively.

4.2.1. The weighted average method

The multi-objective optimization can be expressed in terms of the linear weighted average as

$$\begin{cases} \text{Minimize} & F(t,a) = (1-w)\dfrac{\text{SEA}^*}{\text{SEA}(t,a)} + w\dfrac{P(t,a)}{P^*} \\ \text{s.t.} & w \in [0,1], \\ & 1.4\,\text{mm} \leqslant t \leqslant 3.0\,\text{mm}, \\ & 60\,\text{mm} \leqslant a \leqslant 100\,\text{mm}, \end{cases} \tag{22}$$

where SEA* and P^* are the given normalizing values, which are different for the four different cross-sectional configurations.

By varying weight w in Eq. (22), the Pareto sets for these four cross-sectional layouts are obtained and plotted as in Figs. 9(a)–(d). A clear convexity of all these curves can be observed, which well demonstrates the effectiveness of using the linear weighted method to seek for multi-objective optimization [20]. It is noted that the exploration of the Pareto sets is crucial to fully understand the solution space for the multi-objective optimization problems. The Pareto front provides the designer with a range of optimal solutions for their further decision-making. In all these Pareto plots it is shown that the SEA and peak crushing force criteria strongly compete with each other. To some stage, any further improvement in one objective must sacrifice the other objective. In fact, any point in the Pareto frontier can be an optimum. For example, if the designer wishes to emphasize more on the energy absorption of the structures, a smaller SEA reciprocal should be taken. As a result, the peak crushing force must be compromised and become higher, and *vice versa*.

It should be pointed out that similarly to the single-objective optimization scheme, design variable a is again a constant of 60 mm for all the weighted values of w, which indicates that the shortest side a gives an optimum for not only Max. (SEA) but also Min. (P). However, design variable t shows a large range of variations from the lower bound to the upper bound while varying weight w. Increase in the wall thickness leads to an increase in both SEA and peak crushing force.

Furthermore, it is interesting to compare the results of the single-objective with the multi-objective design, as illustrated in Fig. 9. As expected, it is noted that all the single-objective solutions well locate as single design points on the Pareto frontiers. This implies that the solution from the single-objective schemes can be an optimum for the given selection of primary and secondary objectives. Nevertheless, the designer may have no chance to compare it with other possible solutions unless she/he varies the constraint level. On the other hand, the linear weighted multi-objective design by using the weighted method could generate a full set of Pareto solutions as in Fig. 9. This is that, after the functional constraint in the single-objective problem was removed and the secondary criterion is presented in a form of objective, one could obtain either a higher SEA or a lower peak crushing force than those yielded from the single-objective optimizations. As long as the weight for the

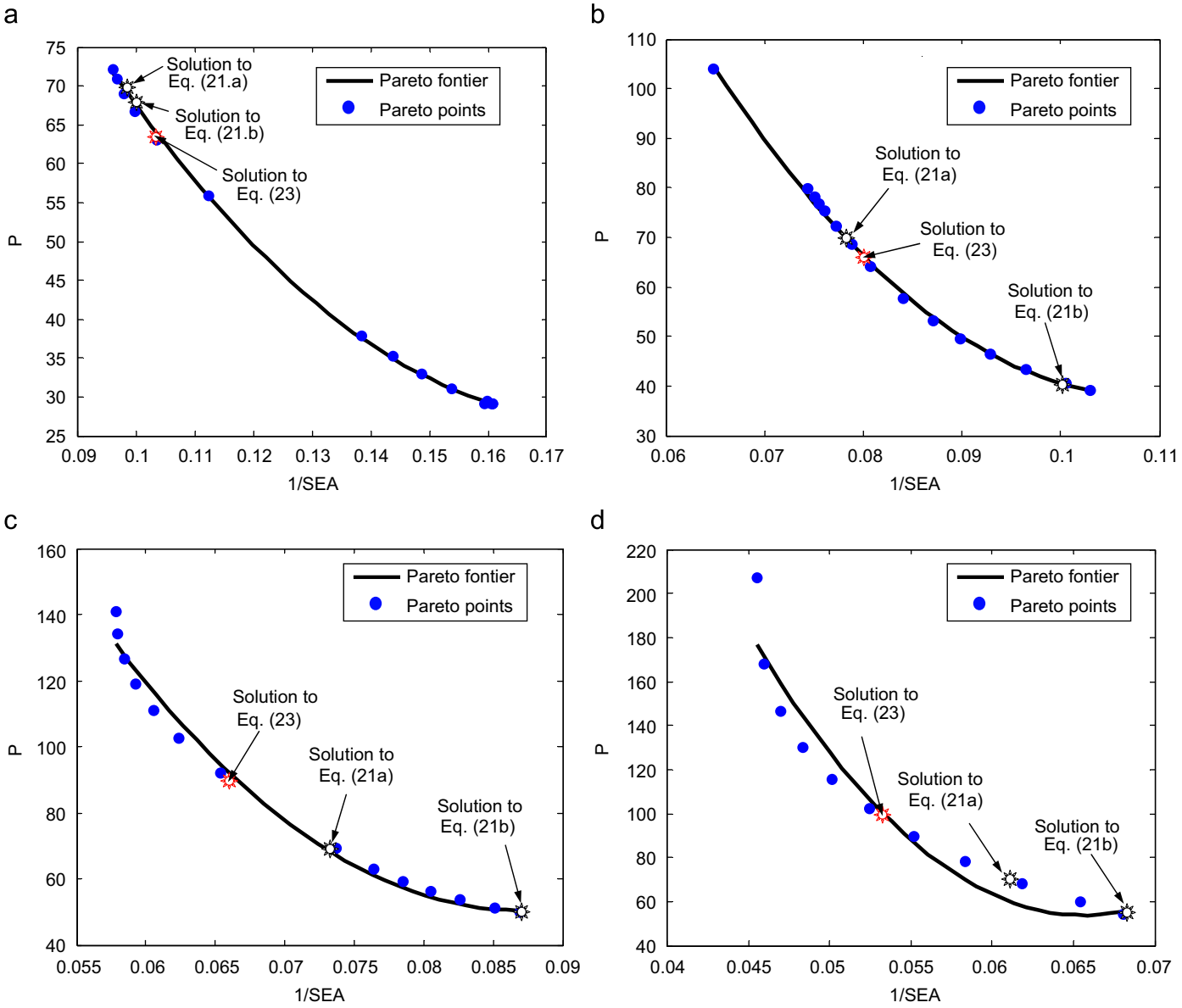

Fig. 9. Pareto spaces for multi-objective optimization. (a) Single cell; (b) double cell; (c) triple cell and (d) quadruple cell.

secondary objective is not too heavy, the emphasis will still be mainly placed on the primary objective and it can thus be optimized to a better value. However, when the weight for the secondary objective becomes comparable with that for the primary objective, the criteria in the multi-objective design can become worse than those in the single-objective design. The examples well reflect the different natures of these two different design problems.

4.2.2. The geometrical average method

In this scheme, the cost function of relative efficiency of each objective is constructed in terms of a geometrical average as

$$\begin{cases} \text{Maximize} & F_g(t,a) = \sqrt{d_{\text{SEA}} d_P} \\ \text{s.t.} & 1.4\,\text{mm} \leqslant t \leqslant 3.0\,\text{mm}, \\ & 60\,\text{mm} \leqslant a \leqslant 100\,\text{mm}, \end{cases} \tag{23}$$

$$d_{\text{SEA}} = \frac{\text{SEA}(t,a) - \text{SEA}^{\text{L}}}{\text{SEA}^{\text{U}} - \text{SEA}^{\text{L}}}, \tag{24}$$

$$d_P = 1 - \frac{P(t,a) - P^{\text{L}}}{P^{\text{U}} - P^{\text{L}}}, \tag{25}$$

where SEA^{L}, SEA^{U} and P^{L}, P^{U} represent the minimum and maximum SEA and peak crushing force, respectively. In fact, this method changes multi-objective problem to a single-objective problem by formulating a special cost function.

The efficiency cost function $F_g(t,a)$ *vs* design variables t and a are plotted for all the four configurations as in Fig. 10, in which one can see that the single , double and triple cells are of very similar cost function shapes, while the quadruple cell shows a different pattern due to the presence of a cruciform at the center.

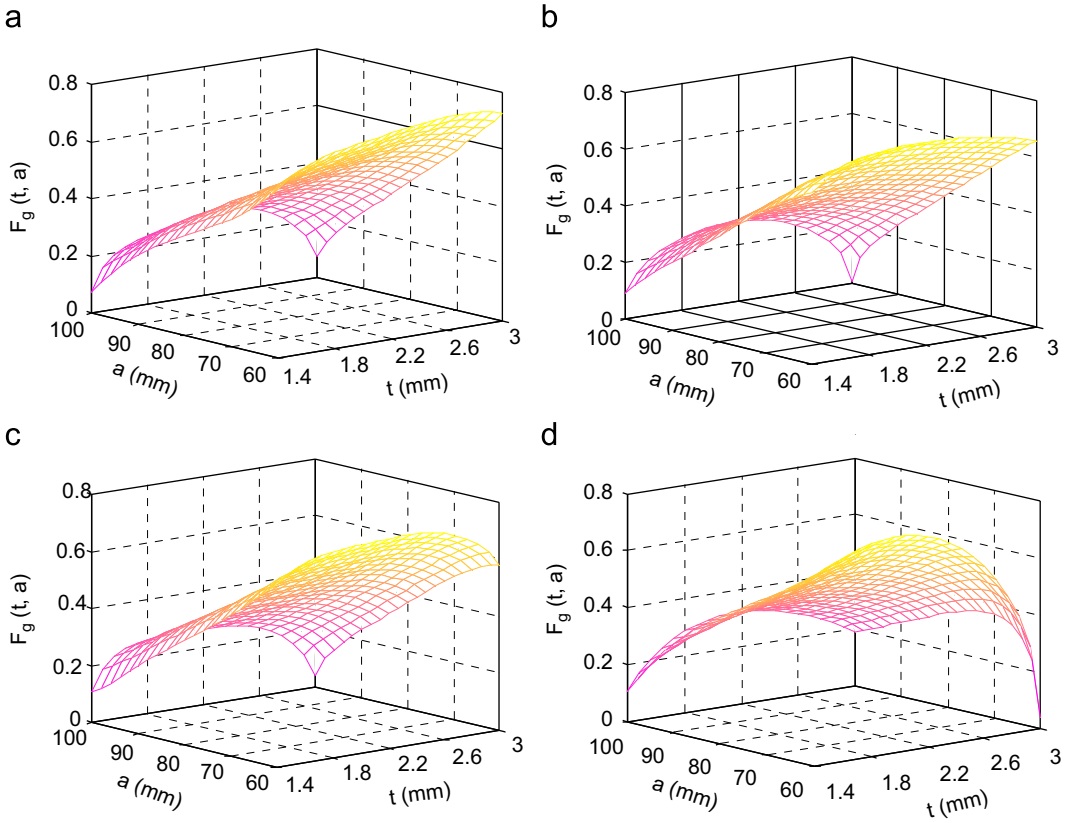

Fig. 10. Surfaces of efficiency coefficient functions $F_g(t,a)$ *vs* design variables. (a) Single cell; (b) double cell; (c) triple cell and (d) quadruple cell.

Table 4
Optimization results by using efficiency coefficient method

Type of cross-section	Optimal design variables (mm)	Cost function $F_g(t,a)$	Relative efficiency d_{SEA}	Relative efficiency d_P	SEA (kN)	P (kJ/kg)
Single cell	$t = 2.71$, $a = 60$	0.7477	0.9022	0.6196	9.77	63.62
Double cell	$t = 2.15$, $a = 60$	0.7158	0.6698	0.7650	12.53	66.18
Triple cell	$t = 2.30$, $a = 60$	0.7365	0.7530	0.7202	15.06	88.95
Quadruple cell	$t = 1.98$, $a = 60$	0.7582	0.7631	0.7533	18.87	99.03

By maximizing the efficiency cost functions $F_g(t,a)$ for all the four different columns, the optimization results are summarized in Table 4. The values of respective efficiency coefficients (d_{SEA}, d_P) and the overall cost functions $F_g(t,a)$ signify the extent that each objective function approaches its corresponding ideal value. The larger the values of d_{SEA}, d_P and $F_g(t,a)$, the better the designs. From Table 4 one can know that the relative optimal efficiency of all the four configurations are in a range of 67–90% for the SEA objective and 62–76% for the peak crushing force objective, respectively.

Due to the presence of the cruciform in the quadruple-cell section, the deformation pattern and energy absorption characteristics are much more complicated than those corner and T-shaped joints presented in the other three columns [33]. As a result, the objective functions and optimization results of the quadruple-cell column are somehow different from those of the other three columns, as summarized in Tables 2 and 4 and Fig. 10.

To observe the relationship between this geometrical average scheme and the weighted average scheme, these optimal results are also plotted in Fig. 9. It can be seen that these optimal results also signify special points in the Pareto frontiers. Moreover, all these solutions to Eq. (23) are different from those solutions to the single-objective optimization points defined in Eqs. (21a) and (21b).

5. Concluding remarks

The sizes of thin-walled multi-cell sectional structures are optimized through two classes of design problems

of the single-objective and multi-objective optimizations. Two different design criteria, namely maximizing specific energy absorption (SEA) and minimizing peak crushing force, are taken into account in this study. The comparative studies are presented for different sectional configurations in terms of the different design criteria.

In terms of polynomial basis functions, the FEA results are fit to the nonlinear response functions for these two different design objectives in the single-, double-, triple- and quadruple-cell configurations, respectively. The influences of sectional widths and wall thicknesses on SEAs and peak crushing forces are also shown through the plots of the response surfaces, which demonstrate a sizeable merit of design optimization in the given domain. The optimal parameters are sought for different criteria by using constrained nonlinear optimization algorithm. An insightful study into the optimization generates some new understanding in the design of multi-cell sectional beams. From the designs of maximizing SEA with a constant peak crushing force as constraint, it is noted that the more the number of cross-sectional cells, the higher the maximum SEA. However, in the design of minimizing peak crushing force with the SEA constraint, there is no regularity being seen for the peak crushing force objective.

The multi-objective design problem is formulated in terms of a linear weighting average scheme and a geometrical average scheme. By varying the weights in the former, the convex Pareto frontiers that consist of multiple solutions can be obtained for all the four sectional layouts, which demonstrated its effectiveness. Using this method, the multi-objective design allows the different criteria being emphasized differently. The examples indicated that these two objectives of SEA and peak crushing force compete with each other strongly. In the Pareto curve, it is clearly shown that any further improvement in one objective must worsen the other objective function. The geometrical average method, on the other hand, generates a single solution to a given relative efficiency measure of optimizing both the objectives. It is interesting to note that all those single-objective designs and this geometrical average multi-objective optimization only signify some special points in the Pareto frontiers, which, on the other hand, implies an overwhelming importance of seeking for Pareto frontier in a multi-objective optimization problem.

Acknowledgment

The financial supports from the Program for Changjiang Scholars and Innovative Research Team in University, the National Natural Science Foundation of China (10372029), Key Project of National Natural Science Foundation of China (60635020) and Australian Research Council (DP0558497) are gratefully acknowledged.

Appendix A. Appendix of functions

The full 4th-order response surface functions for SEA and peak crushing force P are given as follows:

Single cell:

$$\begin{aligned}\mathrm{SEA}(t,a) = {} & 70.978 + 62.197t - 4.8398a - 47.597t^2 \\ & + 0.31424ta + 0.084807a^2 \\ & + 13.971t^3 + 0.074224t^2a - 0.0067016ta^2 \\ & - 6.3393\times10^{-4}a^3 - 1.4919t^4 \\ & - 0.012889t^3a + 9.5504\times10^{-5}t^2a^2 \\ & + 2.7242\times10^{-5}ta^3 + 1.7532\times10^{-6}a^4,\end{aligned} \tag{A.1a}$$

$$\begin{aligned}P(t,a) = {} & 280.58 - 31.12t - 14.068a - 21.787t^2 \\ & + 2.8966ta + 0.23838a^2 \\ & + 5.376t^3 + 0.069818t^2a - 0.033113ta^2 \\ & - 0.0017468a^3 - 0.43099t^4 \\ & - 0.013021t^3a + 2.1779\times10^{-4}t^2a^2 \\ & + 1.3198\times10^{-4}ta^3 + 4.6842\times10^{-6}a^4.\end{aligned} \tag{A.1b}$$

Double cell:

$$\begin{aligned}\mathrm{SEA}(t,a) = {} & -150.38 + 97.587t + 5.5617a - 32.98t^2 \\ & - 1.6109ta - 0.085312a^2 \\ & + 5.4831t^3 + 0.32712t^2a + 0.010384ta^2 \\ & + 6.1288\times10^{-4}a^3 - 0.20218t^4 \\ & - 0.038366t^3a - 4.9448\times10^{-4}t^2a^2 \\ & - 3.076\times10^{-5}ta^3 - 1.6588\times10^{-6}a^4,\end{aligned} \tag{A.2a}$$

$$\begin{aligned}P(t,a) = {} & 154.05 + 29.825t - 9.0354a + 0.5035t^2 \\ & - 0.42476ta + 0.18525a^2 \\ & + 7.5708t^3 - 0.52509t^2a + 0.021668ta^2 \\ & - 0.001731a^3 - 0.28646t^4 \\ & - 0.057057t^3a + 0.0049091t^2a^2 \\ & - 1.4931\times10^{-4}ta^3 + 6.1708\times10^{-6}a^4.\end{aligned} \tag{A.2b}$$

Triple cell:

$$\begin{aligned}\mathrm{SEA}(t,a) = {} & 39.491 + 109.12t - 4.1062a - 77.455t^2 \\ & - 0.24304ta + 0.06959a^2 \\ & + 25.146t^3 - 0.098666t^2a - 0.0013955ta^2 \\ & - 5.4512\times10^{-4}a^3 - 2.7676t^4 \\ & - 0.01287t^3a + 0.0011763t^2a^2 \\ & - 1.3342\times10^{-5}ta^3 + 1.7248\times10^{-6}a^4,\end{aligned} \tag{A.3a}$$

$$P(t,a) = 1030.5 + 70.484t - 55.628a + 61.15t^2 - 4.8967ta + 1.13891a^2 - 7.4734t^3 - 1.0627t^2a + 0.096536ta^2 - 0.01042a^3 + 6.0049t^4 - 0.4969t^3a + 0.024597t^2a^2 - 7.8525 \times 10^{-4}ta^3 + 3.7193 \times 10^{-5}a^4. \quad (A.3b)$$

Quadruple cell:

$$SEA(t,a) = 29.379 + 35.325t - 1.4291a + 57.392t^2 - 3.7777ta + 0.067692a^2 - 21.693t^3 + 0.31252t^2a + 0.034485ta^2 - 1.13 \times 10^{-6}a^3 + 1.8783t^4 + 0.057732t^3a - 0.00407t^2a^2 - 6.0754 \times 10^{-5}ta^3 + 2.7084 \times 10^{-6}a^4, \quad (A.4a)$$

$$P(t,a) = 1226.7 - 312.07t - 55.296a + 767.6t^2 - 25.622ta + 1.3731a^2 - 183.63t^3 - 4.1669t^2a + 0.41157ta^2 - 0.0147a^3 + 21.948t^4 + 0.003776t^3a + 0.021991t^2a^2 - 0.0019558ta^3 + 5.6637 \times 10^{-5}a^4. \quad (A.4b)$$

References

[1] Mahmood H, Aouadi F. Characterization of frontal crash pulses. Crashworthiness, occupant protection and biomechanics in transportation systems. ASME 2000;AMD-Vol. 246/BED-Vol. 49:15–22.

[2] Yamazaki K, Han J. Maximization of the crushing energy absorption of tubes. Struct Optim 1998;16:37–46.

[3] Fang H, Rais-Rohani M, Liu Z, Horstemeyer MF. A comparative study of metamodeling methods for multiobjective crashworthiness optimization. Comput Struct 2005;83:2121–36.

[4] Yang RJ, Wang N, Tho Ch, Bobineau JP. Metamodeling development for vehicle frontal impact simulation. J Mech Des 2005;127(5):1014–20.

[5] Wang GG, Shan S. Review of metamodeling techniques in support of engineering design optimization. J Mech Des 2007;129(4):370–80.

[6] Lee SH, Kim HY, Oh IS. Cylindrical tube optimization using response surface method based on stochastic process. J Mater Process Technol 2002;130–131:490–6.

[7] Avalle M, Chiandussi G, Belingardi G. Design optimization by response surface methodology: application to crashworthiness design of vehicle structures. Struct Multidisciplinary Optim 2002;24:325–32.

[8] Chiandussi G, Avalle M. Maximisation of the crushing performance of a tubular device by shape optimization. Comput Struct 2002;80:2425–32.

[9] Kim HS. New extruded multi-cell aluminum profile for maximum crash energy absorption and weight efficiency. Thin-Walled Struct 2002;40:311–27.

[10] Jansson T, Nilsson L, Redhe M. Using surrogate models and response surface in structural optimization—with application to crashworthiness design and sheet metal forming. Struct Multidisciplinary Optim 2003;25:129–40.

[11] Lee TH, Lee K. Multi-criteria shape optimization of a funnel in cathode ray tubes using a response surface model. Struct Multidisciplinary Optim 2005;29:374–81.

[12] Forsberg J, Nilsson L. On polynomial response surfaces and Kriging for use in structural optimization of crashworthiness. Struct Multidisciplinary Optim 2005;29:232–43.

[13] Forsberg J, Nilsson L. Evaluation of response surface methodologies used in crashworthiness optimization. Int J Impact Eng 2006;32:759–77.

[14] Chen WG, Wierzbicki T. Relative merits of single-cell, multi-cell and foam-filled thin-walled structures in energy absorption. Thin-Walled Struct 2001;39:287–306.

[15] Zarei HR, Kroger M. Multiobjective crashworthiness optimization of circular aluminum tubes. Thin-Walled Struct 2006;44:301–8.

[16] Sinha K. Reliability-based multiobjective optimization for automotive crashworthiness and occupant safety. Struct Multidisciplinary Optim 2007;33:255–68.

[17] Liao XT, Li Q, Yang XJ, Zhang WG, Li W. Multiobjective optimization for crash safety design of vehicles using stepwise regression model. Struct Multidisciplinary Optim, 2007, in press, doi:10.1007/s00158-007-0163-x.

[18] Sobieszczanski-Sobieski J, Kodiyalam S, Yang RY. Optimization of car body under constraints of noise, vibration, and harshness (NVH), and cash. Struct Multidisciplinary Optim 2001;22(4):295–306.

[19] Redhe M, Nilsson L. Optimization of the new Saab 9-3 exposed to impact load using a space mapping technique. Struct Multidisciplinary Optim 2004;27(5):411–20.

[20] Athan TW, Papalambros PY. A note on weighted criteria methods for compromise solutions in multi-objective optimization. Eng Optim 1999;27(2):155–76.

[21] Juntikka R, Kleiven S, Hallstrom S. Optimization of single skin surfaces for head injury prevention—a comparison of optima calculated for global versus local injury thresholds. Int J of Crashworthiness 2004;9:365–79.

[22] Qiao PZ, Yang MJ, Mosallam AS. Impact analysis of I-Lam sandwich system for over-height collision protection of highway bridges. Eng Struct 2004;26:1003–12.

[23] Hou SJ, Li Q, Long SY, Yang XJ, Li W. Design optimization of regular hexagonal thin-walled columns with crashworthiness criteria. Finite Elem Anal Des 2007;43:555–65.

[24] Myers RH, Montgomery DC. Response surface methodology. 1st ed. New York: Wiley; 1995. p. 1–10.

[25] Kurtaran H, Eskandarian A, Marzougui D. Crashworthiness design optimization using successive response surface approximations. Comput Mech 2002;29:409–21.

[26] Montgomery DC. Design and analysis of experiments. 5th ed. New York: Wiley; 2001.

[27] Lindman HR. Analysis of variance in experimental design. New York: Springer; 1992.

[28] Hallquist JO. Theoretical manual. California: Livermore Software Technology Corporation; 1998.

[29] Belytschko T, Lin JI, Tsay CC. Explicit algorithms for the nonlinear dynamics of shells. Comput Methods Appl Mech Eng 1984;42:225–51.

[30] Wierzbicki T, Abramowicz W. On the crushing mechanics of thin-walled structures. J Appl Mech 1983;50:727–39.

[31] Abramowicz W, Wierzbicki T. Axial crushing of multicorner sheet metal columns. J Appl Mech 1989;56:113–20.

[32] Chen LZ. Mechanical optimization design methods. Beijing: Metallurgical Industry Press; 2005.

[33] Zhang X, Cheng GD. A comparative study of energy absorption characteristics of foam-filled and multi-cell square columns. Int J Impact Eng 2007;34:1739–52.